



# Influence of agglomeration and aggregation on the photocatalytic activity of TiO<sub>2</sub> nanoparticles

Francesco Pellegrino<sup>a</sup>, Letizia Pellutiè<sup>a</sup>, Fabrizio Sordello<sup>a</sup>, Claudio Minero<sup>a</sup>, Erik Ortel<sup>b</sup>, Vasile-Dan Hodoroaba<sup>b</sup>, Valter Maurino<sup>b,\*</sup>

<sup>a</sup> Department of Chemistry, University of Turin, Turin, Italy

<sup>b</sup> BAM Federal Institute for Materials Research and Testing, Berlin, Germany

## ARTICLE INFO

### Article history:

Received 30 March 2017

Received in revised form 16 May 2017

Accepted 17 May 2017

Available online 23 May 2017

### Keywords:

Titanium dioxide

Nanoparticles

Agglomeration/Aggregation

Photocatalysis

Quantum yield

## ABSTRACT

Particle aggregation and agglomeration influence the optical properties of materials and therefore their ability to absorb and scatter the incoming radiation, also affecting their photocatalytic activity [1–7]. We have studied the correlation between aggregation and photocatalytic activity for titanium dioxide by means of experimental measurements of extinction and photocatalytic activity and calculations of their optical properties (extinction, absorption and scattering cross-sections). This approach can be adopted to quantitatively assess the quantum yields of the heterogeneous photocatalytic systems. The study was performed on TiO<sub>2</sub> PC105 Cristal ACTIV™, made of aggregated (and agglomerated) primary particles of anatase. The size of the aggregates has been reduced with ultra-sonication. Aqueous suspensions of the obtained materials were characterized by measuring the optical properties (UV-vis extinction), the sizing properties (DLS) and the photocatalytic activity (degradation of phenol under standard conditions). The extinction and absorption spectra of the suspensions were derived from the calculated coefficients, considering also the size distributions measured with DLS, and revealed that light absorption is maximized when particle aggregation and agglomeration are avoided, while diffusion of the incoming radiation dominates when large aggregates and agglomerates are present. The present paper represents a valuable approach to the accurate and reproducible measurement of the photocatalytic activity of TiO<sub>2</sub> nanoparticles suspensions, thus allowing a more reliable comparison of the properties of different materials.

© 2017 Elsevier B.V. All rights reserved.

## 1. Introduction

The growing problem about water decontamination from organic pollutants has led to the research of methods being able to obtain better results on the wastewater treatments, possibly decreasing the utilization of chemical reagents and reducing energy waste. A promising key is the oxidation of the pollutants, possibly up to their complete mineralization [8,9]. Among the advanced oxidation processes (AOPs), titanium dioxide heterogeneous photocatalysis is one of the most promising [10–13].

In this kind of process, a suspension or a supported layer of TiO<sub>2</sub> is exposed to UV radiation, or to sunlight. The irradiation promotes an electron from the valence to the conduction band, producing an electron-hole couple ( $\text{h}^+$ ,  $\text{e}^-$ ) which can migrate to the surface inducing the formation of other reactive species on the photocatalyst surface (surface-trapped holes) and resulting in

the redox initiated transformation of different kinds of organic contaminants [14,15]. The photocatalyzed conversion of organic species has been deeply investigated [9,15]. The photogenerated species interact with the organic substrates depending on their initial oxidation state and the nature of their substituents [16]. The reaction rate is determined by chemical parameters such as the pH of the suspension, the nature of the substrate and the presence of species that can affect the photoactivity directly (as  $\text{Cl}^-$ ) or indirectly by surface adsorption [17], and physical parameters such as the specific surface area, the size, the aggregation and the agglomeration of the particles, which could affect the optical properties of titanium dioxide [1–7,18]. Experimental investigations indicate an optimal size of the TiO<sub>2</sub> particles that maximizes the rates of the photocatalytic oxidation [16–20]. In the studies using slurries the light absorption of the solid cannot be separated from scattering, therefore the analysis of kinetic information and the acquisition of kinetic parameters that are independent on the reactor geometry, size, and form of illumination become very difficult [21] or even impossible. The values of the scattering and absorption coefficients of suspensions, as well as the evaluation of the

\* Corresponding author.

E-mail address: [valter.maurino@unito.it](mailto:valter.maurino@unito.it) (V. Maurino).

local volumetric rate of photon absorption, have been subjected to several studies [22]. This is important for the standardization of photocatalytic materials, as they are commercialized [23]. The problem of particle aggregation and agglomeration, which is often overlooked, together with considerations about aggregate size, has been addressed by Bahnemann group in two recent papers [24,25]. Their findings evidenced how particle agglomeration influences photoactivity and light absorption, and how the interplay between degraded substrate, catalysts employed and aggregation degree lead to different scenarios. It is indeed possible to find increase or decrease of photoactivity due to different agglomeration level depending on the experimental conditions. These findings witness that further research into this field is worth to be conducted, and our contribution focus in the direction of a better fundamental understanding of the effects of aggregation on light absorption, scattering and photodegradation activity of TiO<sub>2</sub> powders.

Here we employed both experimental and theoretical approaches to demonstrate that the formation of agglomerates and aggregates (for definitions of aggregate and agglomerate, see Supporting Info) of NPs causes a change in the optical properties of TiO<sub>2</sub> suspensions, resulting in the decrease of the fraction of the absorbed light. Furthermore, the agglomeration/aggregation may cause the formation of new surface states at the level of contact between particles, resulting in a change of the photon absorption and of the quantum yield, that is not directly related to the primary NPs properties. These effects on the optical properties can lead to an incorrect assessment of the photoactivity. Our approach allows us to estimate the photocatalytic activity of nanoparticles taking into account aggregation and agglomeration phenomena, which cannot be avoided in nanoparticle suspensions.

The approach used here relies on two assumptions/conditions: 1.- the suspensions of TiO<sub>2</sub> the use of dilute aggregate/agglomerate suspensions, in order to be in the single scattering regime (checked by verifying the validity of the Lambert-Beer law); 2. The de-aggregation of TiO<sub>2</sub> Cristal PC105 does not change the surface properties of the nanometric primary particles.

## 2. Experimental

### 2.1. Reagents and materials

Phenol (purity grade >99%) was purchased from Sigma-Aldrich, formic acid (85%) from Carlo Erba, acetonitrile (analytical grade >99.5%) from Sigma-Aldrich. Titanium dioxide Cristal ACTiVTM PC105 (anatase) was provided from CRISTAL. From the pristine PC105 material two other materials were obtained through ultrasonication treatment of different duration 8 and 16 h with an immersion sonifier (400 W Branson Sonifier 450, duty cycle 0.5) in aqueous solution of ammonia (0.5 M, TiO<sub>2</sub> loading of 10 g L<sup>-1</sup>). A treatment with 6 M HCl in a microwave digester (START, MILESTONE) was required to remove the metallic Ti released from the sonifier tip. Same acid treatment was also performed on the pristine material. The materials thus obtained were dialyzed in dialysis membrane with pore size <6–8000 Da against Milli-Q water to remove HCl. The dialyzed suspensions were frozen and lyophilized. The three materials were identified as: US00 (not sonicated), US08 (8 h sonication) and US16 (16 h sonication). The three materials shown only the anatase phase (see Supplementary Data Fig. S3).

### 2.2. Photocatalyst characterization

Dimensional and shape characterization was performed with Dynamic Light Scattering and Scanning Electron Microscopy. Dynamic Light Scattering measurements were carried out with an ALV NIBS (not invasive back scattering) apparatus (ALV, Langen

Germany), equipped with a correlator mod ALV5000, on 10 mg L<sup>-1</sup> TiO<sub>2</sub> suspensions at pH = 3 (HClO<sub>4</sub>). Data analysis on the scattered light autocorrelation function was carried out with the Contin regularization algorithm, to obtain decay time and translational diffusion coefficient distributions. Conversion of translational diffusion coefficients to hydrodynamic radius r<sub>H</sub> of the agglomerates/aggregates is done with the Stokes-Einstein equation. The scanning electron microscope (SEM) employed in this study was a Zeiss Supra 40 SEM (Zeiss, Oberkochen, Germany) equipped with a Schottky field emitter and, additionally to the standard Everhart-Thornley detector, with a high-resolution, *InLens* detector. Hence, high-resolution SEM imaging of the sample surface morphology at the nanometer scale is possible. This type of microscopy is suitable to get access to the size and shape of individual nanoparticles (NPs), also for strongly aggregated/agglomerated TiO<sub>2</sub> NPs presented in this study. Usually, for NPs that could be prepared rather separated on a conventional TEM (transmission electron microscopy) grid, the transmission electron microscopy – either as the typical TEM or as the transmission mode SEM, i.e. TSEM – is successfully applied [26–28]. In this work the two imaging modes (i) the surface sensitive *InLens* SEM mode and (ii) TSEM, suited for dimensional measurements, have been carried out on the same field of view on the sample. More details on this methodological and instrumental approach with advantages and disadvantages can be found in literature [27,28]. Extinction measurements in the UV-vis range were carried out with a Varian Cary “100 Scan” spectrophotometer. The extinction of the catalysts was measured on freshly prepared, previously sonicated suspensions (10 mg L<sup>-1</sup>) at pH = 3 (HClO<sub>4</sub>) and 1 cm optical path length. The suspensions were stable during the time scales necessary for the measurements, and the results of repeated measures were reproducible. Suspensions were not stirred during the measures. The specific surface area was evaluated with physical adsorption of N<sub>2</sub> at liquid nitrogen temperature (77 K) with the instrument Micromeritics ASAP 2020. Adsorption isotherms were measured and data were processed by applying the BET method for the determination of the specific surface area and BJH analysis for the determination of mesoporosity. X-ray diffraction (XRD) pattern of the powders were recorded with an Analytical X'Pert Pro equipped with an X'Celerator detector powder diffractometer using Cu K<sub>α</sub> radiation generated at 45 kV and 40 mA. The 2θ range was from 20° to 90° with a step size (°2θ) of 0.01 and a counting time of 0.6 s.

### 2.3. Irradiation experiments

The photocatalytic activity of TiO<sub>2</sub> was evaluated by irradiating the suspensions (loading 10 mg L<sup>-1</sup>; pH = 3) in cylindrical Pyrex glass cells (4 cm diameter, 2.5 cm height, area of 1.26 × 10<sup>-3</sup> m<sup>2</sup>, cut-off 295 nm, 5 ml suspension volume) under two different fluorescent sources: TL 20W/01 RS Narrowband Philips ( $\lambda_{\text{max}} = 310 \text{ nm}$ ) and TLK 40W/05 Philips ( $\lambda_{\text{max}} = 365 \text{ nm}$ ). Substrate absorption at these wavelengths is negligible. Incident radiant power and incident photons rate were measured in the range 290–400 nm with an Oceans Optics USB2000 spectrophotometer equipped with a cosine corrected optical fiber probe, spectroradiometrically calibrated with a NIST traceable DH-2000 CAL UV-vis source (Ocean Optics). The spectroradiometrical data were acquired and processed with the SpectraSuite software (Ocean Optics). The initial concentration of phenol was 1.0 mM. Time profiles of phenol decay were obtained as average of three irradiation runs.

### 2.4. Analytical determinations

HPLC determination of phenol has been carried out with an Agilent Technologies HPLC chromatograph 1200 Series equipped with

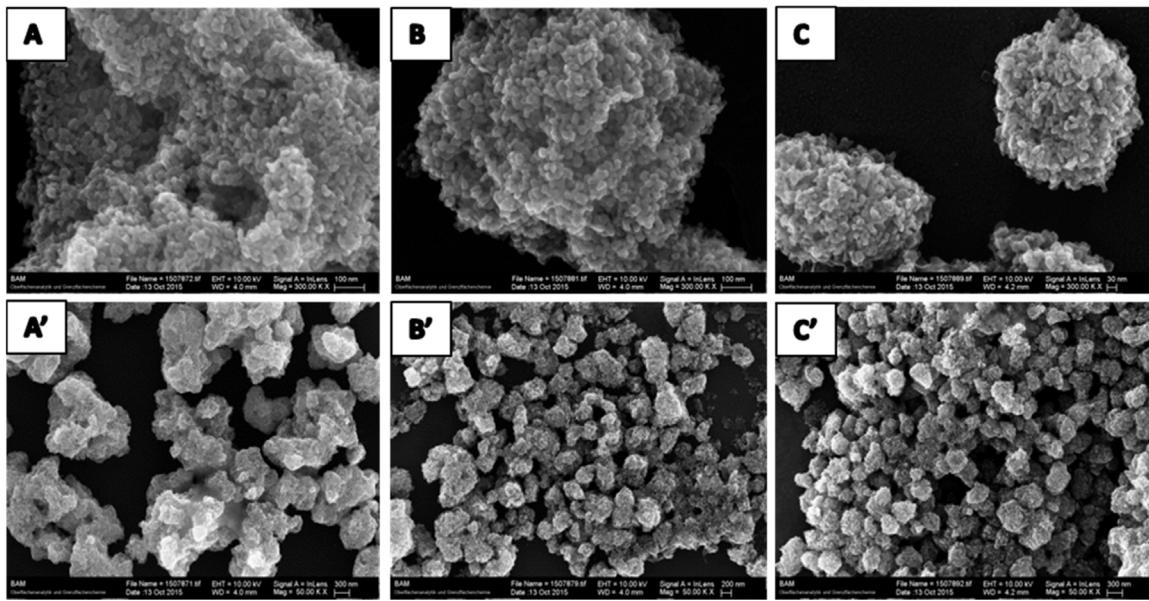


**Fig. 1.** SEM micrographs of the three materials. TOP: A. US00; B. US08; C. US16 (scale bar = 100 nm; magnification = 300 k). BOTTOM: A'. US00; B'. US08; C'. US16 (A' and C' = 300 nm; B' = 200 nm; magnification = 50 k).

a diode array detector, binary gradient high-pressure pump and an automatic sampler. Isocratic elution was carried out with a mixture of 15/85 acetonitrile/formic acid aqueous solution (0.05% w/v), flow rate  $0.2 \text{ ml min}^{-1}$ , injection volume  $20 \mu\text{l}$ . The column used was a Kinetex C18 150-2 (150 mm length, 2 mm diameter Phenomenex), packed with  $2.6 \mu\text{m}$  core-shell stationary phase.

## 2.5. Methodology for the calculation of the extinction spectra: program and building geometries

The code used for the calculation of extinction, absorption and scattering cross sections of spherical NP clusters is MSTM (Multiple-Sphere T Matrix) version 3.0 (2013), a parallelizable program written in Fortran-90 developed by D.W. Mackowski. The algorithm used by programmers applies the method of the T matrix to compute the extinction and scattering coefficient in the framework of the Mie theory [29–32], the results can be considered accurate to the truncation error of the expansion of the vector spherical wave function (VSWF) used to represent the fields. The input data are the geometry of the agglomerates/aggregates and the material optical constants (complex index of refraction). The optical constants of anatase were obtained from the digital library of the Wollam software for spectroscopic ellipsometry Complete EASE (Fig. S1). The MSTM code was run using a cluster of 20 Intel(R) Xeon(R) CPU E5-2680 v2 @ 2.80GHz processors; we performed computations with the option “random orientation” and incident plane wave as radiation source. Since experimental spectra were collected in aqueous suspension, the refractive index of the medium was kept at 1.35. With the “new\_run” option we were able to compute extinction, scattering and absorption cross-sections [33] in the whole UV-vis spectrum with a single input file. Examples of input files, NPs cluster geometry and output files are provided in Supporting Information. Calculated extinction and absorption spectra of aqueous suspensions of agglomerates/aggregates, as well as the fractions of the incoming light absorbed, scattered or transmitted, can be computed from extinction, scattering and absorption cross-sections (see Supporting Information for details) [33]. Because we used dilute suspensions, the single scattering regime is followed and the contribution of the single aggregate/agglomerate to the

total extinction is additive (extinction proportional to the number concentration of aggregates, validity of Beer-Lambert law).

## 3. Results and discussion

### 3.1. Electron microscopy – SEM

SEM micrographs show that PC105 is constituted of anatase primary NPs having size around 20–30 nm, joined to constitute agglomerates/aggregates of the order of hundreds of nanometers with well-developed porosity and a certain degree of polydispersity of shape and size, both for the single NPs and the agglomerates/aggregates. These dimensions are also confirmed by PC105 characterizations published elsewhere using Scherrer analysis of XRD data [34]. A quite accurate assessment of the individual, primary NPs in the external layer of the agglomerates/aggregates is possible thanks to the surface sensitive *InLens* imaging mode (see Fig. 1). The SEM micrographs of the three materials demonstrate the reduction of the agglomerates/aggregates size with the increase of the ultrasonication treatment time (Fig. 1).

Even for agglomerates/aggregates which are electron transparent at 20 kV, the distinction between aggregates and agglomerates and their quantitative determination is a rather impossible task, due to the fact that these are two extreme cases and there is a continuity of the interactions strength between weak adhesion forces and sintering of NPs. In the case of aggregates, the resulting NPs external surface area should be significantly smaller than the sum of surface areas of the individual NPs [35]. Surface areas may be accessed with BET measurements. In our case the increase of specific surface area after ultrasonic treatment is limited (see later). Moreover, the surface texture of the two ultrasonicated materials is quite similar to the untreated one (Fig. 1). As a consequence, ultrasonication reduces the sizes of aggregates/agglomerates by splitting them in zones where the NPs are loosely bound, without strong modification of specific surface areas and surface properties. In conclusion, this type of material is a good model in order to evaluate the  $\text{TiO}_2$  photoactivity as a function of the NPs agglomeration/aggregation level and not of the nature of the primary NPs.

**Table 1**

Physical-chemical properties of the pristine and deaggregated/deagglomerated materials.

Material Name	R <sub>h</sub> (nm) by DLS	Std Dev	BET SSA (m <sup>2</sup> g <sup>-1</sup> )	BJH Mesoporosity (cm <sup>3</sup> g <sup>-1</sup> )	Crystallographic Phase
US00	275	18.6	81 ± 4.0	0.38 ± 0.02	Anatase
US08	184.1	22.9	86 ± 4.5	0.38 ± 0.02	Anatase
	21.1 <sup>a</sup>	0.9			
US16	140.6	13.3	88 ± 4.5	0.37 ± 0.02	Anatase
	28.5 <sup>a</sup>	1.6			

<sup>a</sup> Small mode obtained after the ultrasonication.

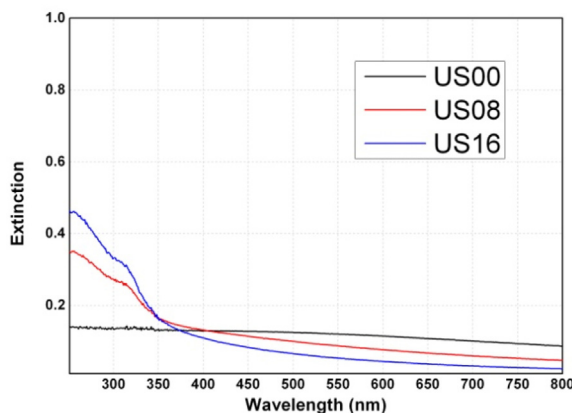


**Fig. 2.** UV-vis extinction spectra of untreated and ultrasonicated PC105 water suspensions at 10 mg L<sup>-1</sup>.

### 3.2. Specific surface area (SSA) and size distribution

**Table 1** reports a comparison of the hydrodynamic radii (mode(s) and their standard deviation), specific surface areas and mesoporosities of the three materials. The main effect of the ultrasonic treatment is on the hydrodynamic radius, whereas the SSA and mesoporosity are very similar. Ultrasonication reduced the agglomerates/aggregates hydrodynamic radius from 275 nm to 185 nm (8 h ultrasonication) and 140 nm (16 h ultrasonication). Moreover, for the ultrasonicated materials a bimodal size distribution was observed (**Table 1**, Fig. S2). The accessible specific surface area showed a limited increase (less than 10%) and mesoporosity was not significantly affected. Ultrasonication did not expose isolated mesopores, whose presence can be excluded. As stated in the preceding paragraph, the limited increase in specific surface area suggests the fragmentation of aggregates/agglomerates does not involve strongly sintered NPs. Superficial disaggregation of loosely bound clusters composed of few NPs give rises of the small mode in the size distribution of ultrasonicated materials.

### 3.3. UV-vis extinction spectra of suspensions

UV-vis spectra of material suspensions (loading 10 mg L<sup>-1</sup>) are reported in **Fig. 2**. The spectra are strongly dependent on the ultrasonication time. Specifically, there is an increase of the extinction in the UV range with increasing ultrasonication time, and a decrease in the Vis region. Obviously, these changes in the extinction spectra of the TiO<sub>2</sub> NPs suspensions are due to a reduction of the agglomerate/aggregates size. The anatase band gap (E<sub>g</sub> = 3.2 eV) limits the electronic transition in the ultraviolet (wavelengths less or equal 380 nm), consequently the extinction in the visible range is due to scattering phenomena only. Conversely, in the UV range the extinction is due to both scattering and absorption of light. This suggests that the agglomerate/aggregate size reduction clearly decreases the scattering in the visible region and possibly increases the absorption in the UV, directly affecting the photocatalytic activity of titanium dioxide.

### 3.4. Calculated spectra

Experimental extinction spectra do not allow the measurement of the absorbed radiation and QY. Evaluation of the scattered and absorbed fraction of the incident radiation can be carried out with the calculation of the scattering and absorption cross-sections of particles/agglomerates/aggregates, if suspensions are in the single scattering regime. The code MSTM allows the calculation of extinction and scattering coefficient for clusters of spherical NPs. Taking into account that from SEM micrographs primary NPs are in the range of 20–30 nm diameter, agglomerates/aggregates of PC105 were simulated building spheroidal clusters of spheres of 25 nm diameter with hexagonal close packed (hcp) structure. From the mesoporosity data, it can be estimated a 60% volume fraction of voids inside the agglomerates/aggregates. We modeled these voids randomly removing spheres inside the cluster. The US00 material US00 was modeled with a spheroidal cluster 275 nm radius. The two ultrasonicated materials have a bimodal distribution of the hydrodynamic radii, therefore their spectra were modeled as a weighted sum of the calculated spectra of a big cluster (185 nm (US08) and 140 nm (US16)) and a small cubic cluster of eight primary NPs. **Fig. 3** shows all these clusters geometry. Because at low loadings of catalyst (10 mg L<sup>-1</sup>) the NP dispersions are in the single scattering regime, the extinction spectra have been calculated with the calculated C<sub>ext</sub> applying the Lambert-Beer law (additive contribution to the extinction of the single clusters).

The calculated UV-vis extinction spectra (**Fig. 4**) reproduce only qualitatively the experimental spectra of the three materials, i.e., with the decrease of the agglomerates/aggregates size, there is a decrease of the scattering and a raise of the absorption in the UV range, but the matching with the experimental spectra is not perfect, indeed the calculated extinctions are overestimated in the UV and underestimated in the Visible. The materials show polydispersity both at aggregate/agglomerate and primary NPs level. Moreover, primary NPs are not spherical. The modelling of extinction spectra by using monodispersed clusters and primary particles can be only a first approximation. The effect of polydispersity is the smoothing of the experimental spectra with respect of the calculated ones (**Fig. 2** vs **Fig. 4**).

A good fit of the calculated and experimental UV-vis extinction spectra would allow the evaluation of the absorbed radiation fraction, and a reliable estimation of the quantum yields of the photocatalytic process. In order to make a first approximation estimation of the radiation absorbed, we assumed that the ratio between the calculated absorbed and extinguished fraction in the UV region ( $\lambda < 400$  nm) is a good approximation of the same ratio for the PC105 aggregates/agglomerates. This is partly justified by the fact that, in the UV region, these ratios calculated for single spheres and for the clusters of same radius are very similar.

The estimate of the experimental absorbed fraction is reported in **Fig. 5**. As expected, absorbed fraction increases with the decrease of aggregate/agglomerate radius. It is noteworthy that absorbed fractions differ significantly under 320 nm, whereas under 350 nm the differences are less significant. A qualitative explanation of these differences lies in the penetration depth of the radiation inside the agglomerates/aggregates. With the optical constants

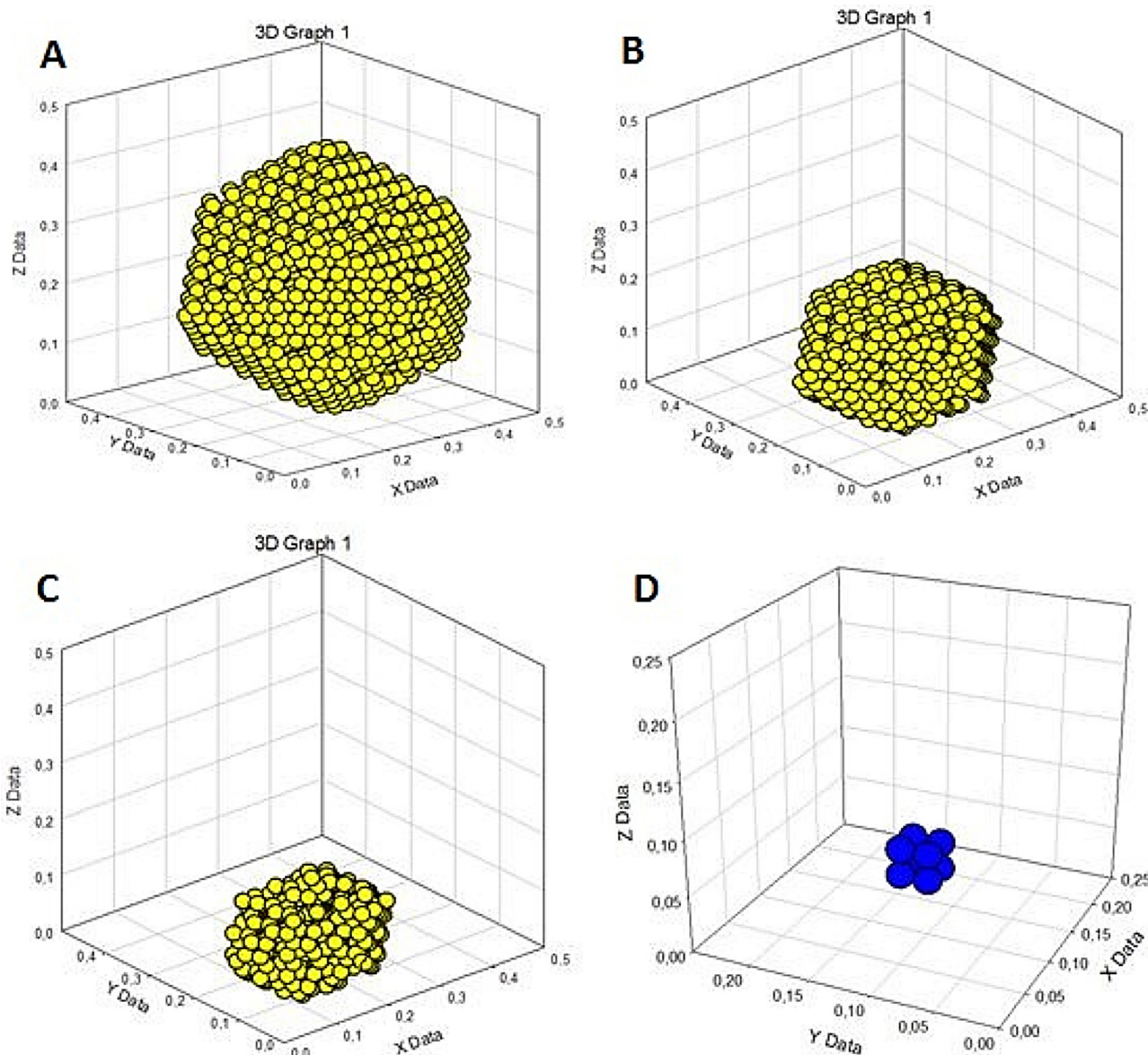


**Fig. 3.** Cluster geometries used to simulate the extinction and scattering coefficients of PC105 aggregates/agglomerates: A US00; B US08; C US16; D cubic cluster of eight primary particles.

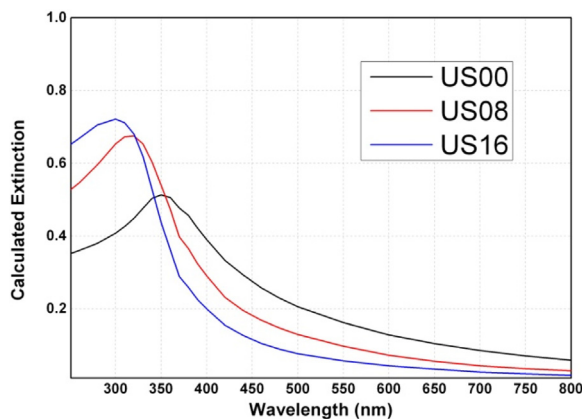


**Fig. 4.** Calculated UV-vis extinction spectra for 10 mg/L suspensions of the clusters of sphere used to simulate the PC105 materials.

reported in the SI, going from 365 to 310 nm the decadic absorption coefficient of bulk anatase increase of ten times. Accordingly, for bulk anatase the penetration depths at 310 and 365 nm are roughly 40 and 400 nm. At 365 nm, the aggregates/agglomerates of all three PC105 samples are nearly fully illuminated, whereas at 310 nm the portion of the aggregates/agglomerates that it is not illuminated, hence not photo-catalytically active, is higher for bigger clusters.

### 3.5. Photocatalytic activity

The photocatalytic activity of the three samples was evaluated monitoring the oxidative phototransformation of phenol [17]. A comparison between the degradation curves of the three materials is shown in Fig. 6 and in Supporting Information (Fig. S3) at two different incident radiant powers and two different wavelength (310 and 365 nm). The curves show the  $C/C_0$  ratio as a function of the irradiation time. The decays of phenol concentration with time show first-order kinetics for all the samples within two-three half-lives. This kind of dependence of the concentration on time occurs when

**Table 2**

Incident photons rate and photon absorption rate as functions of the hydrodynamic radius and the wavelength.

Wavelength (nm)	Incident Radiant Power (W m <sup>-2</sup> ) – Range 290–400 nm	Incident photons rate <sup>a</sup> (Ein min <sup>-1</sup> × 10 <sup>-6</sup> ) – Range 290–400 nm	Photon Abs Rate (Ein min <sup>-1</sup> × 10 <sup>-6</sup> ) – Range 290–400 nm		
			US00–280 nm	US08–175 nm	US16–135 nm
365	13	3.65	0.101	0.125	0.138
310	11	2.62	0.288	0.449	0.536
365	6	1.73	0.049	0.061	0.068
310	5	1.15	0.128	0.199	0.237

<sup>a</sup> Refers to the area of the irradiation cell window, equal  $1.52 \times 10^{-3} \text{ m}^2$ .

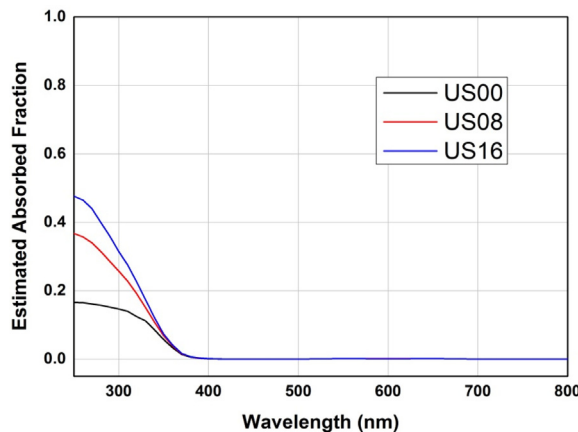


**Fig. 5.** Estimated absorbed radiation fraction for the PC105 materials (see text for details).

the photo-catalytic process is not controlled by the adsorption of the substrate [18,36].

Data in Fig. 6 and in Fig. S4 were fitted to an exponential decay and the initial disappearance rates of phenol calculated and reported in Fig. 7. The phenol abatement rate as a function of the agglomerates/aggregates size varies scarcely at 365 nm, while significantly increases with decreasing agglomerates/aggregates size at 310 nm, irrespective of the incident radiant power employed.

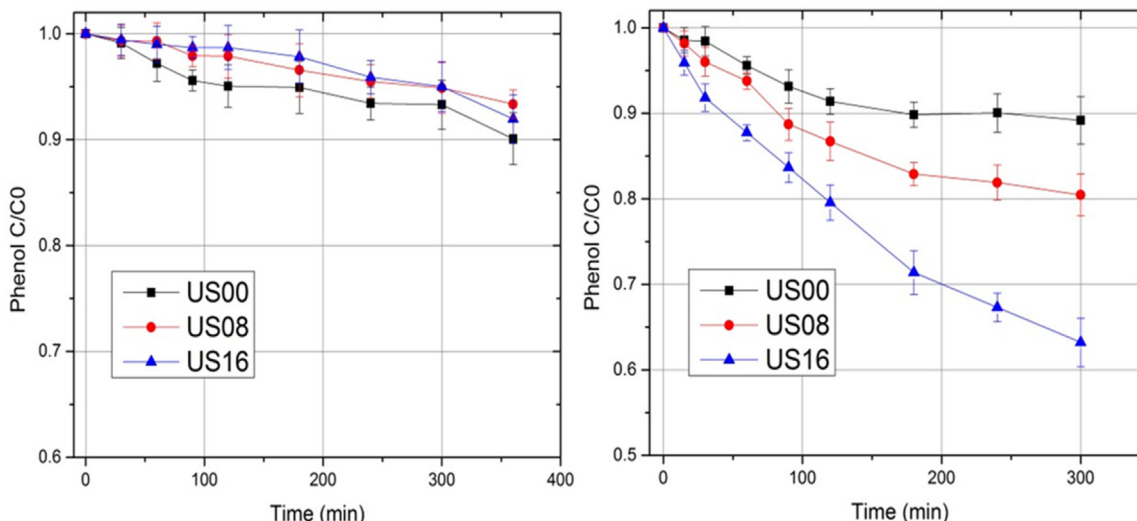


**Fig. 6.** Degradation curves of phenol with a concentration of  $10 \text{ mg L}^{-1}$  for the materials studied and under an irradiation of 365 nm ( $13 \text{ W m}^{-2}$ ) (left) and 310 nm ( $11 \text{ W m}^{-2}$ ) (right).

### 3.6. Quantum yields estimate

The fraction of radiation absorbed allows estimating the quantum yields (QYs) of the photocatalytic processes, as the ratio of the initial degradation rates and the number of absorbed photons per unit time. Table 2 reports incident radiant power, incident photons and the estimation of photon absorption rates for all experiments. Under 310 nm irradiation the photon absorption rate increases significantly (up to 100%) with decreasing agglomerate/aggregate size. Instead, under 365 nm irradiation the increase in absorbed photons is more limited, with just a slight rise (up to 40%) with decreasing size. The estimates of the photon absorption rates and the measured degradations rate allowed us to carry out an educated guess of the QY for the three materials at the irradiation wavelengths employed (Fig. 8). The values found are quite low, but in line with those reported in literature [18,29,36–38].

With 365 nm irradiation, where the penetration depth of the radiation is of the order of aggregates size, no significant variation in the QY and degradation rate is observed as a function of photocatalysts agglomeration/aggregation.

QY dependence on agglomerate/aggregate size is quite different at 310 nm irradiation. At low size the QY are the double of those observed at 365 nm, with a significant decrease with the increase of agglomerate/aggregate size. As noted in the preceding paragraph, the penetration depth of the 310 nm radiation is of the order of 40 nm, explaining the relevant decrease of absorbed radiation with the increase of size. The behaviour of QY at 310 nm can be attributed to two factors with opposite effects. Low penetration depth of the radiation generates electron-hole pair in closer proximity to the surface of aggregates. Due to hole diffusion lengths in  $\text{TiO}_2$  of the order of nanometers [39], this effect increases the

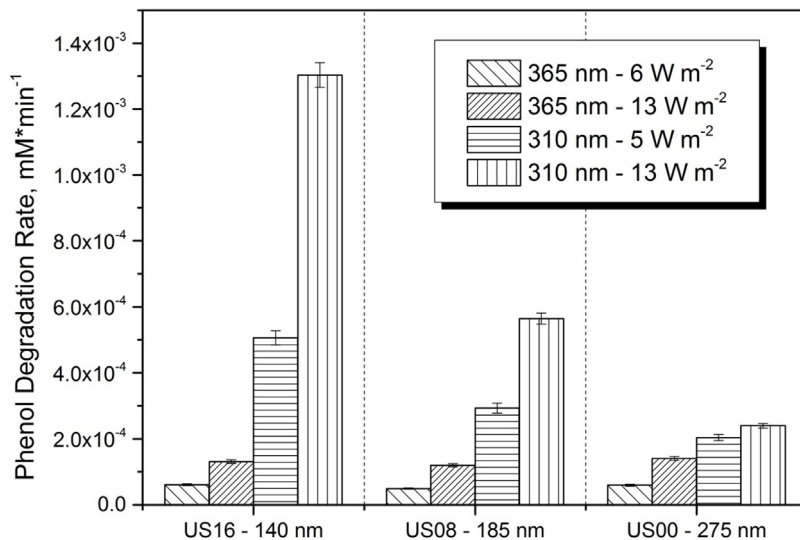


**Fig. 7.** Comparison between the initial degradation rates of phenol for the three materials ( $10 \text{ mg L}^{-1}$ ), with the two different irradiation wavelengths and at different incident radiant powers.

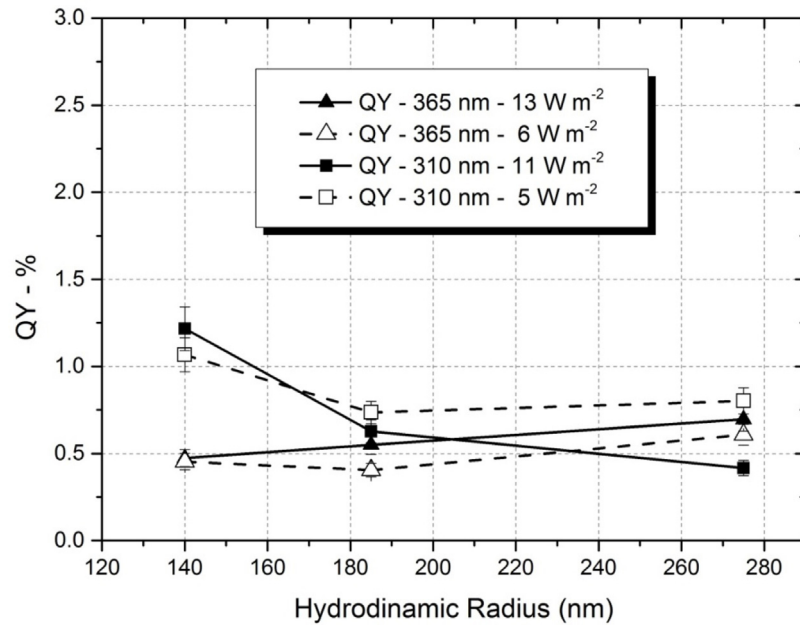


**Fig. 8.** Estimated quantum yields and photon absorption rates for the three materials under the two different wavelengths; incident radiant power: 11 and  $5 \text{ W m}^{-2}$  for the irradiation at 310 nm; 13 and  $6 \text{ W m}^{-2}$  for the irradiation at 365 nm.

fraction of holes that reach the external layer of the aggregates. However, the increase in size decreases the surface to volume ratio of the aggregates, thereby favouring surface recombination.

#### 4. Conclusions

Deaggregation/Deagglomeration of  $\text{TiO}_2$  PC105, combined with *in silico* evaluation of extinction and absorption coefficient of aggregates, allows setting up a good model system to study the influence of aggregation/agglomeration on  $\text{TiO}_2$  NPs photocatalytic activity. Phenol degradation rate and estimated QY at low photocatalyst loading (single scattering regime) depend strongly on the photocatalyst agglomerate/aggregate size when incident radiation is of  $\lambda < 320\text{--}330 \text{ nm}$ , where the absorbed fraction significantly varies with size. The effect is primarily due to a low penetration depth of the radiation inside the aggregates/agglomerates, limiting

the volume fraction of the aggregates/agglomerates that is irradiated and, hence, photo-catalytically active. The significant increase of QY at low aggregate size at 310 nm, compared to irradiation at higher wavelength (365 nm), can be attributed to the generation of electron-hole pair in closer proximity to the surface of aggregates, due to hole diffusion lengths in  $\text{TiO}_2$  of the order of nanometers [39]. Concerning the *in silico* evaluation of the spectra of the  $\text{TiO}_2$  NP agglomerates/aggregates suspensions, it is possible to conclude that the calculated extinction reproduces semi-quantitatively the experimental spectra allowing the estimation of the QY. The present work demonstrates that the photocatalyst aggregation and agglomeration affect/control the optical properties of  $\text{TiO}_2$  determining the amount of absorbed radiation and, therefore, control/affect the photoactivity. In order to do a proper comparison of the photoactivity of NP aggregated and agglomerated materials, the control of agglomeration/aggregation is mandatorily required,

or at least the penetration depth of the radiation should be higher than the agglomerate/aggregate size and the suspensions must be diluted (single scattering).

Better matching between experimental and calculated extinction spectra could be achieved with the improvement of the geometrical model of the NP agglomerates/aggregates, accounting for polydispersity of the photo-catalyst at agglomerate/aggregate and primary NPs levels.

## Acknowledgements

The authors are grateful to CRISTAL for the material (Cristal ACTiV<sup>TM</sup> PC105) provided.

This work was supported by SETNanoMetro, EU Project, FP7-NMP-2013 LARGE-7. Project number: 604577

## Appendix A. Supplementary data

Supplementary data associated with this article can be found, in the online version, at <http://dx.doi.org/10.1016/j.apcatb.2017.05.046>.

## References

- [1] Y. Park, W. Kim, D. Monllor-Satoca, T. Tachikawa, T. Majima, W. Choi, Role of interparticle charge transfers in agglomerated photocatalyst nanoparticles: demonstration in aqueous suspension of dye-sensitized TiO<sub>2</sub>, *J. Phys. Chem. Lett.* 4 (2013) 189–194.
- [2] C.Y. Wang, R. Pagel, J.K. Dohrmann, D.W. Bahnemann, Antenna mechanism and deaggregation concept: novel mechanistic principles for photocatalysis, *C.R. Chim.* 9 (2006) 761–773.
- [3] H. Lin, C.P. Huang, W. Li, C. Ni, S.I. Shah, Y.-H. Tseng, Size dependency of nanocrystalline TiO<sub>2</sub> on its optical property and photocatalytic reactivity exemplified by 2-chlorophenol, *Appl. Catal. B: Environ.* 68 (2006) 1–11.
- [4] T. Cordero, J.M. Chovelon, C. Duchamp, C. Ferronato, J. Matos, Surface nano-aggregation and photocatalytic activity of TiO<sub>2</sub> on H-type activated carbons, *Appl. Catal. B: Environ.* 73 (2007) 227–235.
- [5] Zs. Pap, V. Danciu, Zs. Cegléd, A. Kukovecz, A. Oszko, A. Dombi, K. Mogyorosi, The influence of rapid heat treatment in still air on the photocatalytic activity of titania photocatalysts for phenol and monuron degradation, *Appl. Catal. B: Environ.* 101 (2011) 461–470.
- [6] K. Mogyorosi, N. Balazs, D.F. Sranko, E. Tombacz, I. Dekany, A. Oszko, P. Sipos, A. Dombi, The effect of particle shape on the activity of nanocrystalline TiO<sub>2</sub> photocatalysts in phenol decomposition. Part 3: the importance of surface quality, *Appl. Catal. B: Environ.* 96 (2010) 577–585.
- [7] D. Friedmann, C. Mendive, D. Bahnemann, TiO<sub>2</sub> for water treatment: parameters affecting the kinetics and mechanisms of photocatalysis, *Appl. Catal. B: Environ.* 99 (2010) 398–406.
- [8] D. Vione, C. Minero, V. Maurino, A.E. Carlotti, T. Picatonotto, E. Pelizzetti, Degradation of phenol and benzoic acid in the presence of a TiO<sub>2</sub>-based heterogeneous photocatalyst, *Appl. Catal. B: Environ.* 58 (2005) 79–88.
- [9] O. Legrini, E. Oliveros, A.M. Braun, Photochemical processes for water-treatment, *Chem. Rev.* 93 (1993) 671–698.
- [10] S.G. Kumar, L.G. Devi, Review on modified TiO<sub>2</sub> photocatalysis under UV/visible light: selected results and related mechanisms on interfacial charge carrier transfer dynamics, *J. Phys. Chem. A* 115 (2011) 13211–13241.
- [11] Y. Ohko, D.A. Tryk, K. Hashimoto, A. Fujishima, Autoxidation of acetaldehyde initiated by TiO<sub>2</sub> photocatalysis under weak UV illumination, *J. Phys. Chem. B* 102 (1998) 2699–2704.
- [12] M.R. Hoffmann, S.T. Martin, W. Choi, D.W. Bahnemann, Environmental applications of semiconductor photocatalysis, *Chem. Rev.* 95 (1995) 69–96.
- [13] A.L. Linsebigler, G. Lu, J.T. Yates, Photocatalysis on TiO<sub>2</sub> surfaces: principles, mechanisms, and selected results, *Chem. Rev.* 95 (1995) 735–758.
- [14] O.M. Alfano, D. Bahnemann, A.E. Cassano, R. Dillert, R. Goslich, Photocatalysis in water environments using artificial and solar light, *Catal. Today* 58 (2000) 199–230.
- [15] Bahnemann Robertson, J.M.C. Robertson, Wood, Photocatalytic Detoxification of Water and Air, Environmental Photochemistry Part II, Springer, Berlin Heidelberg, 2005.
- [16] E. Pelizzetti, C. Minero, Role of oxidative and reductive pathways in the photocatalytic degradation of organic compounds, *Colloids Surface A Physicochem. Eng. Aspects* 151 (1999) 321–327.
- [17] C. Minero, G. Mariella, V. Maurino, D. Vione, E. Pelizzetti, Photocatalytic transformation of organic compounds in the presence of inorganic ions. 2. Competitive reactions of phenol and alcohols on a titanium dioxide-fluoride system†, *Langmuir* 16 (2000) 8964–8972.
- [18] C. Minero, D. Vione, A quantitative evalution of the photocatalytic performance of TiO<sub>2</sub> slurries, *Appl. Catal. B-Environ.* 67 (2006) 257–269.
- [19] H. Gerischer, Photocatalysis in aqueous solution with small TiO<sub>2</sub> particles and the dependence of the quantum yield on particle size and light intensity, *Electrochim. Acta* 40 (1995) 1277–1281.
- [20] C.C. Wang, Z.B. Zhang, J.Y. Ying, Photocatalytic decomposition of halogenated organics over nanocrystalline titania, *Nanostruct. Mater.* 9 (1997) 583–586.
- [21] A.J. Maira, K.L. Yeung, C.Y. Lee, P.L. Yue, C.K. Chan, Size effects in gas-phase photo-oxidation of trichloroethylene using nanometer-sized TiO<sub>2</sub> catalysts, *J. Catal.* 192 (2000) 185–196.
- [22] C.B. Almquist, P. Biswas, Role of synthesis method and particle size of nanostructured TiO<sub>2</sub> on its photoactivity, *J. Catal.* 212 (2002) 145–156.
- [23] M.A. Grela, A.J. Colussi, Kinetics of stochastic charge transfer and recombination events in semiconductor colloids. Relevance to photocatalysis efficiency, *J. Phys. Chem.* 100 (1996) 18214–18221.
- [24] J. Melcher, N. Barth, C. Schilde, A. Kwade, D. Bahnemann, Influence of TiO<sub>2</sub> agglomerate and aggregate sizes on photocatalytic activity, *J. Mater. Sci.* 52 (2017) 1047–1056.
- [25] I. Ivanova, C.B. Mendive, D. Bahnemann, The role of nanoparticulate agglomerates in TiO<sub>2</sub> photocatalysis: degradation of oxalic acid, *J. Nanopart. Res.* 18 (2016) 187.
- [26] P.-J.D. Temmerman, E. Verleysen, J. Lammertyn, J. Mast, Semi-automatic size measurement of primary particles in aggregated nanomaterials by transmission electron microscopy, *Powder Technol.* 261 (2014) 191–200.
- [27] V.D. Hodoroaba, C. Motzku, T. Mace, S. Vaslin-Reimann, Performance of high-resolution SEM/EDX systems equipped with transmission mode (TSEM) for imaging and measurement of size and size distribution of spherical nanoparticles, *Microsc. Microanal.* 20 (2014) 602–612.
- [28] V.D. Hodoroaba, D. Akcakayiran, D.O. Grigoriev, D.G. Shchukin, Characterization of micro- and nanocapsules for self-healing anti-corrosion coatings by high-resolution SEM with coupled transmission mode and EDX, *Analyst* 139 (2014) 2004–2010.
- [29] Y. Ohko, K. Hashimoto, A. Fujishima, Kinetics of photocatalytic reactions under extremely low-intensity UV illumination on titanium dioxide thin films, *J. Phys. Chem. A* 101 (1997) 8057–8062.
- [30] D.W. Mackowski, M.I. Mishchenko, Calculation of the T matrix and the scattering matrix for ensembles of spheres, *J. Opt. Soc. Am. A-Opt. Image Sci. Vision* 13 (1996) 2266–2278.
- [31] A. Quirantes, A T-matrix method and computer code for randomly oriented, axially symmetric coated scatterers, *J. Quant. Spectrosc. Radiat. Transfer* 92 (2005) 373–381.
- [32] M.I. Mishchenko, L.D. Travis, A.A. Lacis, Scattering, Absorption, and Emission of Light by Small Particles, Cambridge University Press, 2002.
- [33] H.C. Van de Hulst, Light scattering by small particles, *Q. J. R. Meteorol. Soc.* 84 (1958) 198–199.
- [34] C.L. Bianchi, S. Gatto, C. Pirola, A. Naldoni, A. Di Michele, G. Cerrato, V. Crocellà, V. Capucci, Photocatalytic degradation of acetone, acetaldehyde and toluene in gas-phase: comparison between nano and micro-sized TiO<sub>2</sub>, *Appl. Catal. B: Environ.* 146 (2014) 123–130.
- [35] ISO/TS27687:2008, Nanotechnologies—Terminology and Definitions for Nano-objects—Nanoparticle, Nanofibre and Nanoplate, ISO International Organization for Standardization, Geneva, Switzerland.
- [36] C. Minero, Kinetic analysis of photoinduced reactions at the water semiconductor interface, *Catal. Today* 54 (1999) 205–216.
- [37] A. Salinaro, A.V. Emeline, J.C. Zhao, H. Hidaka, V.K. Ryabchuk, N. Serpone, Terminology, relative photonic efficiencies and quantum yields in heterogeneous photocatalysis. Part II: experimental determination of quantum yields (technical report), *Pure Appl. Chem.* 71 (1999) 321–335.
- [38] N. Serpone, A. Salinaro, Terminology, relative photonic efficiencies and quantum yields in heterogeneous photocatalysis. Part I: suggested protocol (technical report), *Pure Appl. Chem.* 71 (1999) 303–320.
- [39] P. Salvador, Hole diffusion length in n-TiO<sub>2</sub> single crystals and sintered electrodes: photoelectrochemical determination and comparative analysis, *J. Appl. Phys.* 55 (1984) 2977–2985.